GEOPHYSICS, VOL. 79, NO. 6 (NOVEMBER-DECEMBER 2014); P. U15–U23, 13 FIGS.
10.1190/GEO2014-0112.1

Horizon-based semiautomated nonhyperbolic velocity analysis

Bo Zhang[1], Tao Zhao[1], Jie Qi[1], and Kurt J. Marfurt[1]

ABSTRACT

With higher capacity recording systems, long-offset surveys are becoming common in seismic exploration plays. Long offsets provide leverage against multiples, have greater sensitivity to anisotropy, and are key to accurate inversion for shear impedance and density. There are two main issues associated with preserving the data fidelity contained in the large offsets: (1) nonhyperbolic velocity analysis and (2) mitigating the migration/NMO stretch. Current nonhyperbolic velocity analysis workflows first estimate moveout velocity V_{nmo} based on the offset-limited gathers, then pick an effective anellipticity η_{eff} using the full-offset gathers. Unfortunately, estimating V_{nmo} at small aperture may be inaccurate, with picking errors in V_{nmo} introducing errors in the subsequent analysis of effective anellipticity. We have developed an automated algorithm to simultaneously estimate the nonhyperbolic parameters. Instead of directly seeking an effective stacking model, the algorithm finds an interval model that gives the most powerful stack. The searching procedure for the best interval model was conducted using a direct, global optimization algorithm called *differential evolutionary*. Next, we applied an antistretch workflow to minimize stretch at a far offset after obtaining the optimal effective model. The automated velocity analysis and antistretch workflow were tested on the data volume acquired over the Fort Worth Basin, USA. The results provided noticeable improvement on the prestack gathers and on the stacked data volume.

INTRODUCTION

Velocity analysis applied on CMP gathers is usually based on computing the coherence of moveout-corrected gathers using zero-offset times and a suite of trial stacking velocities. Velocity analysis is one of the most important and interpreter-time-consuming tasks in seismic processing. The accuracy of velocity analysis depends on (1) the resolution of the velocity spectra, (2) the accuracy of the selected equation in approximating the kinematic behaviors of the reflection events, and (3) the skill and experience of the data processor.

Semblance is perhaps the most commonly used coherency measurements for the velocity spectra (Taner and Koehler, 1969; Neidell and Taner, 1971). Swan (2001) is one of the first researchers to develop a high-resolution velocity-spectra algorithm that accounts for amplitude variation with offset (AVO). Larner and Celis (2007) improve the resolution and reliability of the velocity spectra by just using selected subsets of crosscorrelation rather than all possible ones in the gathers. To minimize the effect of AVO phenomenon that exists in prestack gathers, Fomel (2009) proposes a generalized "AB semblance" that is particularly attractive for velocity analysis of class II AVO anomalies in which the polarity of the reflections changes. To further improve the resolution of semblance-based velocity spectra, Luo and Hale (2010) introduce a weighting function that slightly increases the cost of calculation but is still comparable with that of conventional semblance. Biondi and Kostov (1989) introduce high-resolution velocity spectra by using an eigenstructure method rather than semblance. Key and Smithson (1990) also use eigenstructure analysis, which is based on covariance measurement of NMO-corrected traces, to get higher velocity spectrum and locate the reflection events. Kirlin (1992) deduces the relationship between semblance and eigenstructure velocity estimators. The eigenstructure-based estimators have higher resolution but greater computation cost. Sacchi (1998) further improves the resolution of velocity spectra by integrating a bootstrap method in the covariance computation. Unfortunately, his computational cost is also very expensive.

The approximated kinematic behaviors of the moveout correction for P-wave reflection traveltime are defined by either hyperbolic (Dix, 1955) or nonhyperbolic equations (Thomsen, 1986; Alkhalifah and Tsvankin, 1995; Alkhalifah, 1997). The hyperbolic traveltime approximation equation is based on the assumption of a homogeneous isotropic or elliptically anisotropic layer-cake model

Manuscript received by the Editor 7 March 2014; revised manuscript received 14 July 2014; published online 7 October 2014.
[1]The University of Oklahoma, ConocoPhillips School of Geology and Geophysics, Norman, Oklahoma, USA. E-mail: bo.zhang-1@ou.edu; tao-zhao@ou.edu; jie.qi@ou.edu; kmarfurt@ou.edu.

and needs to be restricted to small aperture (the offset-to-depth ratio $2h/z \leq 1.0$). As offset increases, we often encounter nonhyperbolic moveout in isotropic (Bolshykh, 1956, Taner and Koehler, 1969; de Bazelaire, 1988) and anisotropic media (Alkhalifah, 1997, 2011; Fomel and Stovas, 2010). Ignoring the anisotropy in prestack migration will lead to failure to properly correct the moveout of dipping reflectors and cause errors in reflector positioning and focusing. The most common nonhyperbolic equations are fourth-order approximations expressed using three parameters: (1) the two-way, zero-offset traveltime t_0, (2) the short-spread NMO velocity V_{nmo}, and (3) an effective anellipticity η_{eff}. The effective anellipticity combines the effects of long-offset ray bending (the "Snell" effect) as well as intrinsic anisotropy. Alkhalifah (1997) introduces what is now the most commonly used two-step approach for nonhyperbolic velocity analysis, in which the first estimates the NMO velocity on offset-limited truncated gather using hyperbolic NMO correction, followed by estimation of effective anellipticity using the full-offset gathers. Unfortunately, small aperture NMO velocity analysis may be inaccurate. Picking errors in V_{nmo} introduces errors into the subsequent analysis of effective anellipticity.

Conventional velocity analysis (CVA) requires manually picking the peaks of the semblance panel. Such picking is tedious, and a great deal of effort has been invested in attempting to accelerate this process. CVA also requires a great deal of skill and experience. There is no guarantee that the picked RMS velocity represents the true earth model. Erroneous picks of RMS velocity (for example of picking multiple reflections) leads to infeasible interval velocities model. Toldi (1989) proposes one of the first velocity analysis algorithms that avoids manual picking. Instead of directly searching the rms velocity, his algorithm examines a suite of possible interval velocity models, calculates the corresponding rms velocity using the Dix equation, and then estimates the corresponding stacking power. The final product is an interval velocity model that, when converted to a moveout curve, corresponds to the most powerful stacking. His least-squares optimization algorithm is parameterized by layers of equal time thickness without explicitly considering the location of reflection events. Building on the concept of measuring the degree of reflections flattening using an l_1-norm in the τ-p domain, Calderón-Macías et al. (1998) perform automatic velocity analysis to recover the interval velocity model. Van der Baan and Kendall (2002) also invert the model in the τ-p domain and conclude that there exists a family of kinematically equivalent models that exhibit identical moveout curves. Siliqi et al. (2003) obtain dense model parameters by simultaneously picking velocity and anellipticity. Abbad et al. (2009) propose two-step automatic nonhyperbolic velocity analysis using a normalized bootstrapped differential semblance (BDS). They first perform hyperbolic velocity analysis on truncated small-offset data at coarse space to identify events and then implement dense nonhyperbolic velocity analysis about the identified events. The BDS estimator has higher resolution than differential semblance (DS) but can significantly increase the computation cost. Choi et al. (2010) develop an efficient automatic velocity analysis algorithm by using BDS and Monte Carlo inversion.

Most velocity analysis is done in a seismic data-processing services company by professional processors. These velocities are then used to prestack migrate the data. Our goal in this paper is to present a workflow that improves upon these images, giving a residual velocity analysis.

To use the critical information contained in the long-offset data, we need not only to flatten the reflections at far offset using nonhyperbolic traveltime equation but also minimize the stretch typically associated with large aperture. In this paper, we first extend Toldi's (1989) method by adding interval anellipticity as one of the parameters for the model to perform automatic nonhyperbolic analysis based on user-defined horizons. We then follow Zhang et al. (2013) to minimize the stretch at far offset. We apply our technique as a residual velocity analysis workflow to a prestack time-migrated data volume acquired over the Fort Worth Basin (FWB), USA, and show the improvements on the prestack-corrected gathers and final stacked section.

AUTOMATED NONHYPERBOLIC VELOCITY ANALYSIS

There are mainly two issues in performing automatic residual velocity analysis. The first issue is to select a proper traveltime equation. The second issue is to define the objective function as a function of the proposed model. In this paper, we use the well-known nonhyperbolic trajectory (Alkhalifah, 1997). Our model parameters consist of interval velocity v_{nmo} and anellipticity $\eta_{\text{int}}(\tau)$. The objective is to find an interval model that gives the maximum stacking power (semblance). Our optimization engine is a direct, global searching called the *differential evolution* (DE) algorithm.

Traveltime equations

The shifted hyperbola (de Bazelaire, 1988; Castle, 1994) and Alkhalifah-Tsvankin (Alkhalifah and Tsvankin, 1995; Alkhalifah, 1997) approximation are among the most commonly used traveltime equations for nonhyperbolic velocity analysis. Because we wish to perform residual velocity analysis on anisotropic shale reservoirs, we use the Alkhalifah-Tsvankin approximation:

$$t^2(x) = t_0^2 + \frac{x^2}{V_{\text{nmo}}^2} - \frac{2\eta_{\text{eff}}x^4}{V_{\text{nmo}}^2[t_0^2V_{\text{nmo}}^2 + (1+2\eta_{\text{eff}})x^2]}, \quad (1)$$

where t_0 is the two-way traveltime at zero-offset, x is the offset, $V_{\text{nmo}}(t_0)$ is the NMO velocity at small apertures, and η_{eff} is effective anellipticity.

For vertical transverse isotropic (VTI) media, Alkhalifah (1997) deduces the relationship between effective and interval values using the Dix forward equations:

$$V_{\text{nmo}}^2(t_0) = \frac{1}{t_0}\int_0^{t_0} v_{\text{nmo}}^2(\tau)\mathrm{d}\tau, \quad (2)$$

and

$$\eta_{\text{eff}}(t_0) = \frac{1}{8}\left\{\frac{1}{t_0 v_{\text{nmo}}^4(t_0)}\int_0^{t_0} v_{\text{nmo}}^4(\tau)[1+8\eta_{\text{int}}(\tau)]\mathrm{d}\tau - 1\right\}, \quad (3)$$

where $\eta_{\text{int}}(\tau)$ is the instantaneous (interval) anisotropy, and v_{nmo} is the interval NMO velocity given by

$$v_{\text{nmo}}(\tau) = v(\tau)\sqrt{1 + 2\delta(\tau)}, \tag{4}$$

where $v(\tau)$ is the vertical interval velocity and $\delta(\tau)$ is one of the Thomsen's anisotropy parameters (Thomsen, 1986). Note that although equation 1 has higher accuracy than the conventional Dix equation, it is not suitable for velocity analysis when the absolute value of η_{eff} exceeds 0.2. Large values of η_{eff} may result in possibly smoother and lower resolution in η_{int}. Furthermore, equation 1 may introduce up to 2% traveltime error when the aperture is greater than 2.0 (Alkhalifah, 1997).

Differential evolution optimization

Least-squares maximization is usually the optimization engine for automatic velocity analysis (e.g., Toldi, 1989). Classical least-squares requires the Hessian matrix (or approximations of the Hessian using the Jacobian matrix) to define the next search step. Unfortunately, the relationship between the stacking power and a given interval model is highly nonlinear (Toldi, 1989). For this reason, we use an efficient, global search engine called DE, which is described in Appendix A, to obtain the optimal interval velocity and anellipticity model. The advantage of DE is that it avoids any estimation of derivatives but rather requires more computation to generate forward models, and it is more expensive than that of least-squares-based optimization.

The objective function

Toldi (1989) proposes a two-step workflow to conduct automated hyperbolic velocity analysis. First, he calculates the stacking slowness from predicted trial interval slowness models. Then, the algorithm computes the total stacking power of corrected gathers. The model with the greatest stacking power is considered as the best model. We follow Toldi's workflow by extending it to automated nonhyperbolic velocity analysis. Toldi (1989) parameterizes the interval velocity model using equally spaced increments along the t_0-axis. In contrast, because we focus on residual velocity analysis of migrated gathers, we geologically consider our interval model using user-defined horizons. We choose the semblance S as the estimator of stacking power to minimize cost, though eigenstructure methods provide higher resolution (Key and Smithson, 1990; Sacchi, 1998). The objective of our algorithm is to search an interval model $\mathbf{m}$ that gives the maximum semblance value S. And the model $\mathbf{m}$ consists of the interval NMO velocity v_{nmo} and instantaneous (interval) anisotropy η_{int} parameters that are given as

$$\mathbf{m} = (v_{\text{nmo}}, \eta_{\text{int}}) \tag{5}$$

and objective function $Q(\mathbf{m})$

$$Q(\mathbf{m}) = \sum_j \sum_k S(\mathbf{m}, x_j, y_k), \tag{6}$$

where x and y stand for the inline and crossline and indices j and k indicate the index of inline and crossline samples.

Figure 1 illustrates the proposed workflow for automatic nonhyperbolic velocity analysis. Our input data consist of prestack time-migrated CMP gathers, the initial migration velocity, and interpreted horizons. The outputs are flattened gathers, and a model of interval velocity and anellipticity that best flatten the gathers. The prestack gathers are generated from a time-migrated gather that has been subjected to a reverse NMO correction using the migration velocity. The horizons are manually interpreted on an offset-limited stack of the migrated gathers and are used to parameterize the interval model $\mathbf{m}$. The algorithm starts by building an initial interval velocity model from migration velocity and then generates a suite of alternative models in the decision space. Next, the model undergoes DE mutation and crossover to generate a set of new trial interval models and calculate the effective models using equation 2. The algorithm estimates the objective function for each model and better models survive into the next generation. We repeat generating and evaluating the new models until all the reflection events are flattened, or convergence slows down.

MINIMIZE THE STRETCH ASSOCIATED WITH FAR OFFSET

Migration and NMO corrections are conducted sample by sample that results in the well-known decrease of frequency content and amplitude distortion through stretch at far offset. To avoid the effects of serious stretch associated with large offsets, we usually mute the farther offsets based on a user-defined criterion. Muting of large offset not only lowers the stacking power but also reduces

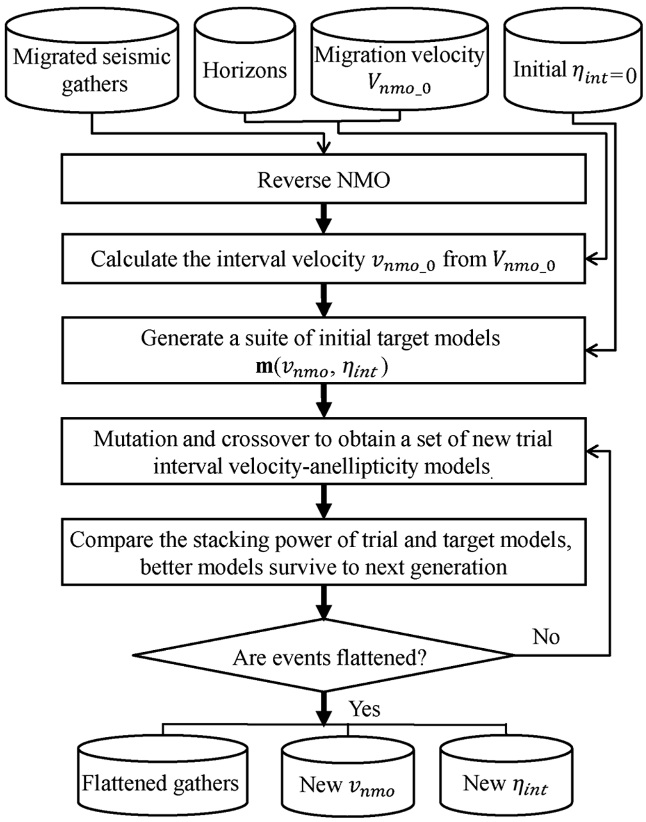

Figure 1. Flowchart showing the automated nonhyperbolic velocity analysis. The model parameters consist of interval NMO velocity and anellipticity. The objective is to find a model that gives the maximum stacking power using a global optimization strategy called DE.

information necessary for accurate prestack inversion of shear impedance and density. Zhang et al. (2013) develop a wavelet-based algorithm named MPNMO (the matching-pursuit-based normal moveout correction) to minimize the stretch at large aperture. Their algorithm first applies reverse NMO correction, which "resqueezes" the migration stretch of the time-migrated gathers and then conducts a wavelet-based NMO correction on the reverse-NMO-corrected gathers. In this paper, we apply their workflow to the time-migrated gathers using the new velocity and anellipticity models. In this manner, resolution is improved first by aligning the data and second by avoiding stretch. Furthermore, the AVO phenomenon that exits in the prestack gathers is well preserved.

APPLICATION

To illustrate the effectiveness of the proposed workflow, we apply it to prestack time-migrated CMP gathers in the FWB, USA. The FWB is a foreland basin and covers approximately 140,000 km^2 in north-central Texas. The target is Mississippian Barnett Shale, which is one of the largest unconventional reservoirs in the world and spreads approximately 73,000 km^2 across the FWB. Although the Barnett Shale (da Silva, 2013) is present in 38 counties in Texas, production is mainly restricted to Denton, Tarrant, Johnson, and Wise counties in the northeastern portion of the FWB. Our survey is located in Wise County and has a maximum offset of 4200 m. The target Barnett Shale lies at approximately 2100-m depth. Figure 2 shows a simplified stratigraphic column of the FWB in Wise County (Montgomery et al., 2005; da Silva, 2013). Note the Barnett Shale lies directly on the easy-to-pick Viola limestone.

Figure 3 is a representative time-migrated CMP gather using the two-term hyperbolic traveltime equation. Note the "hockey-stick-like pattern" and stretch indicated by the white arrows at far offsets. Hockey-stick-like pattern and stretch are harmful for the following processing and prestack inversion. The hockey-stick-like pattern can blur reflection events in the stacked volume whereas the stretch lowers the resolution of shear impedance and inversion volume.

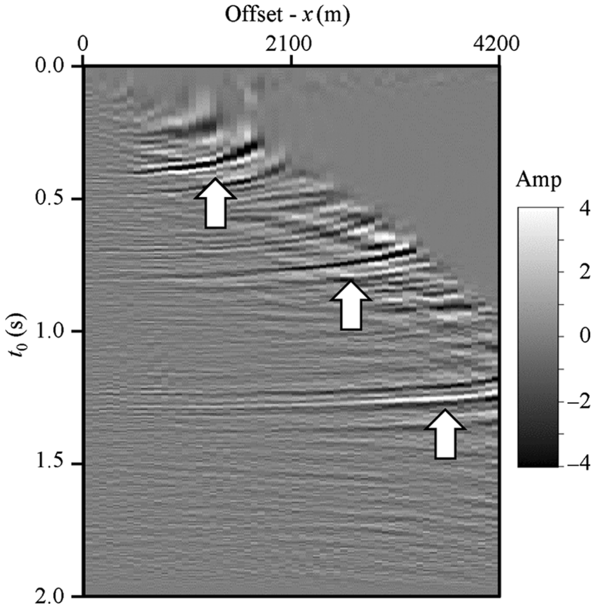

Figure 3. A representative time-migrated CMP gather using the two-term hyperbolic traveltime equation and the migration velocity shown in Figure 6. Note the hockey-stick-like pattern and stretch indicated by the white arrows at far offset.

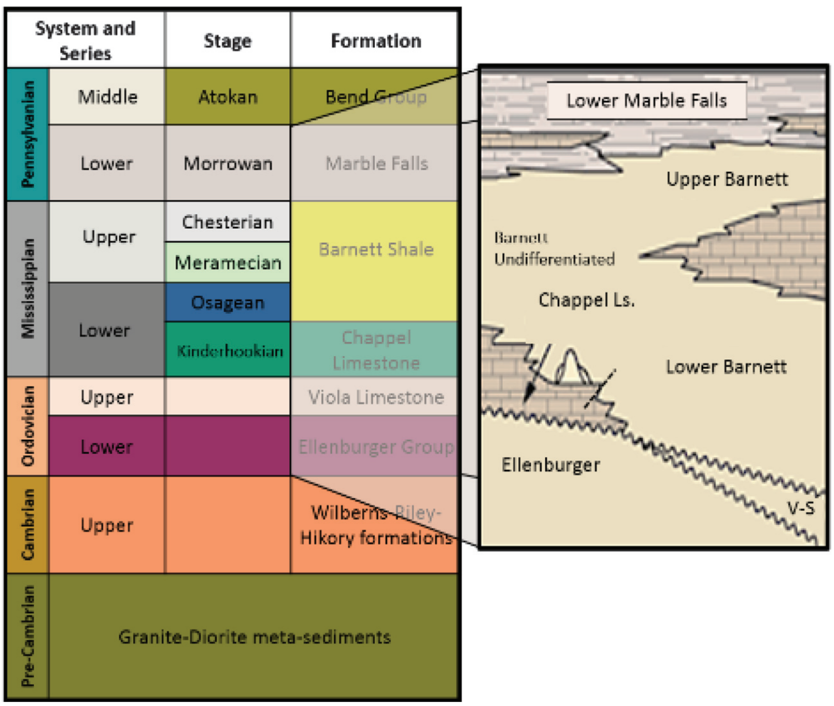

Figure 2. Simplified stratigraphic column of the FWB in Wise County (da Silva, 2013). The Barnett Shale lies between the Marble Falls and Viola Limestone in our survey area.

Usually, seriously stretched data are muted out (Figure 4) based on a user-defined muting criterion. In this example, we allow wavelets to stretch no more than 130%. Figure 5 shows a prestack gather after applying reverse NMO correction on the gather shown in Figure 3. The rms migration velocity (Figure 6a) comes from performing hyperbolic velocity analysis on coarse-grid (20×20) supergathers. The migration velocity is then converted to interval velocity (Figure 6b) as one of the inputs for our algorithm. Figure 7 shows the horizons used for parameterizing the model. They are interpreted on

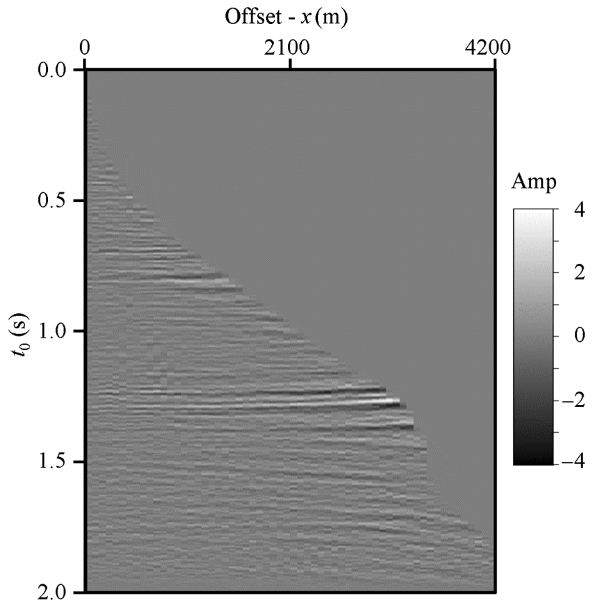

Figure 4. The gather shown in Figure 3 after muting. The wavelet is not allowed to stretch more than 130%, resulting in the loss of information in the far offset.

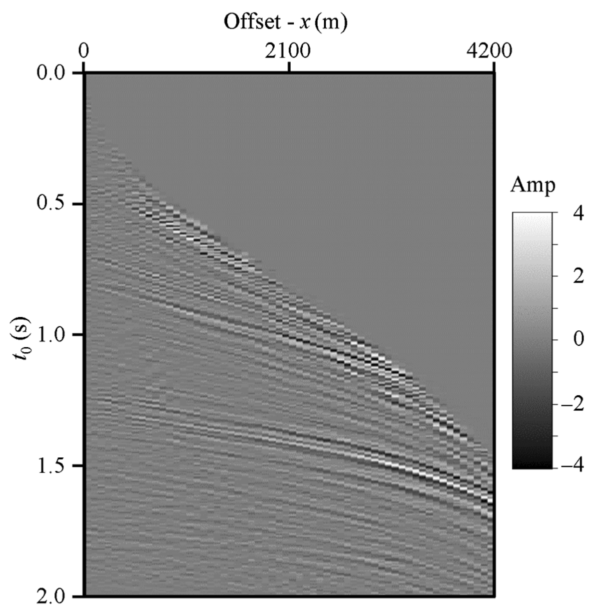

Figure 5. The gather shown in Figure 3 after applying reverse NMO. This gather serves as input to automatic nonhyperbolic velocity analysis.

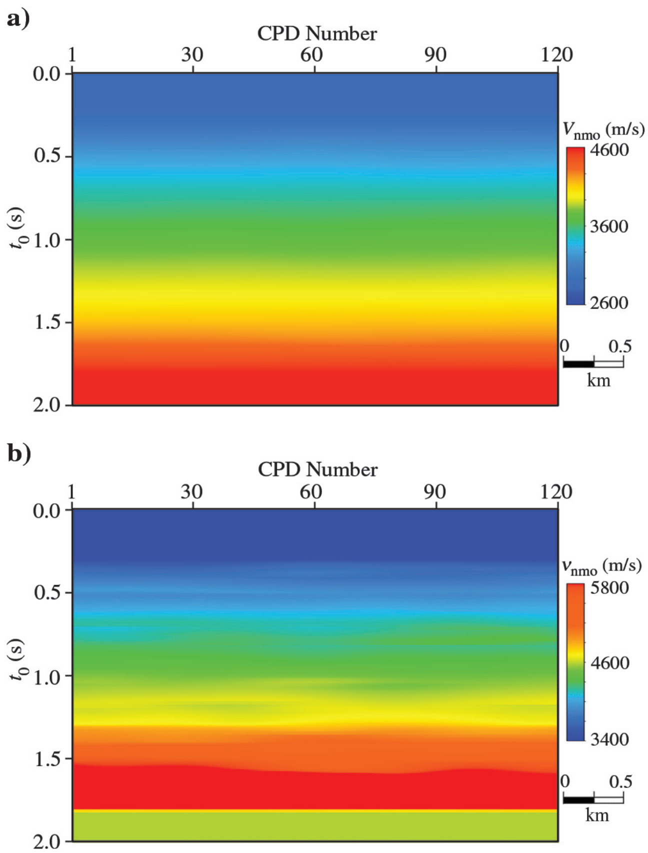

Figure 6. Velocity analysis results performed on the coarse grid (20×20) supergathers. (a) The rms velocity from hyperbolic velocity analysis on the offset-truncated gathers and (b) interval velocity converted from the rms velocity. This interval velocity is used for generating the initial target interval velocity. The initial interval anellipticity is set to zero.

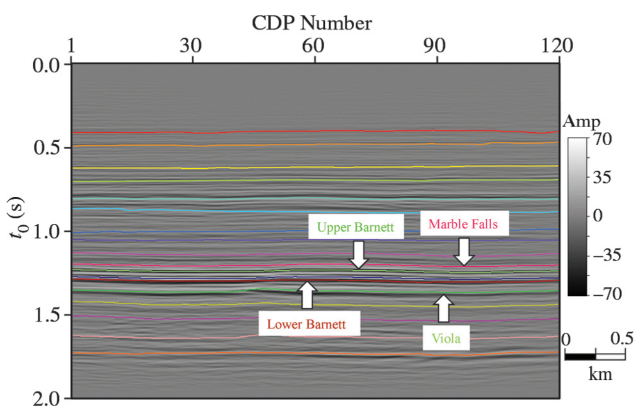

Figure 7. Horizons used in parameterizing the model. We interpreted these 18 horizons on the stacked volume of near-offset time-migrated gathers (Figure 4). The named horizons are tied to wells. Unnamed horizons provide further constraints.

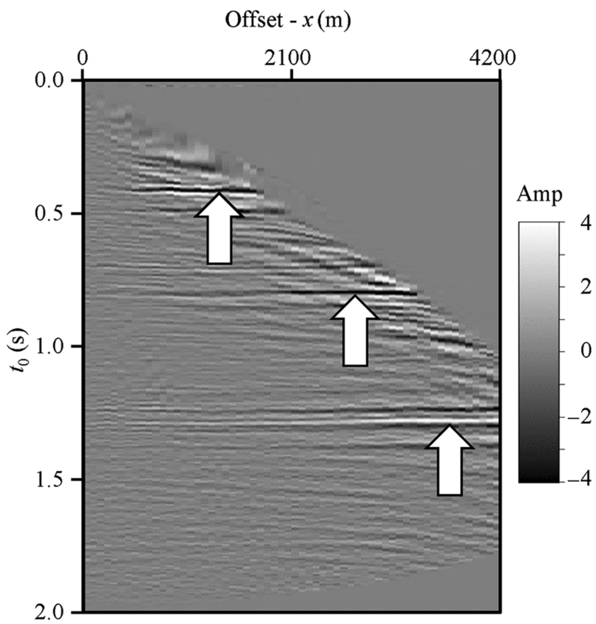

Figure 8. Flattened representative gathers using the workflow shown in Figure 1. Note the hockey-stick-like pattern is gone but not the stretch.

the stacked volume, which just uses the near-offset data of the time-migrated gather (Figure 4). During each generation, we only update the interval slowness and anellipticity values located at those horizons. Other interval model values are interpolated using values on the horizons.

To automatically flatten the gather shown in Figure 5 without picking, we apply the workflow shown in Figure 1 to obtain the corrected results (Figure 8). The initial interval anellipticity η_{int} is set to zero, and the maximum absolute value of corresponding η_{eff} is limited to 0.2 during the optimization. The maximum absolute deviation of interval velocity from the initial model is not permitted to more than 20%. Figure 9a and 9b shows the optimal interval NMO velocity and anellipticity. The corresponding optimal rms velocity and effective anellipticity are, respectively, shown in Figure 9c and 9d. Compared to the initial velocity model, the optimized interval NMO and rms velocity have higher resolution. The differences between initial and optimized velocities are caused by (1) the isotropic assumption compensating for the anellipticity (Abbad et al., 2009) and (2) the initial velocity analysis performed on coarse-grid supergathers having lower lateral resolution. Some correlations are observed between the inverted model and the geology features in the stacked section. For example, the velocity pattern (high-low-high) indicated by the white arrows in Figure 9a correlates to the Marble Falls Limestone–Upper

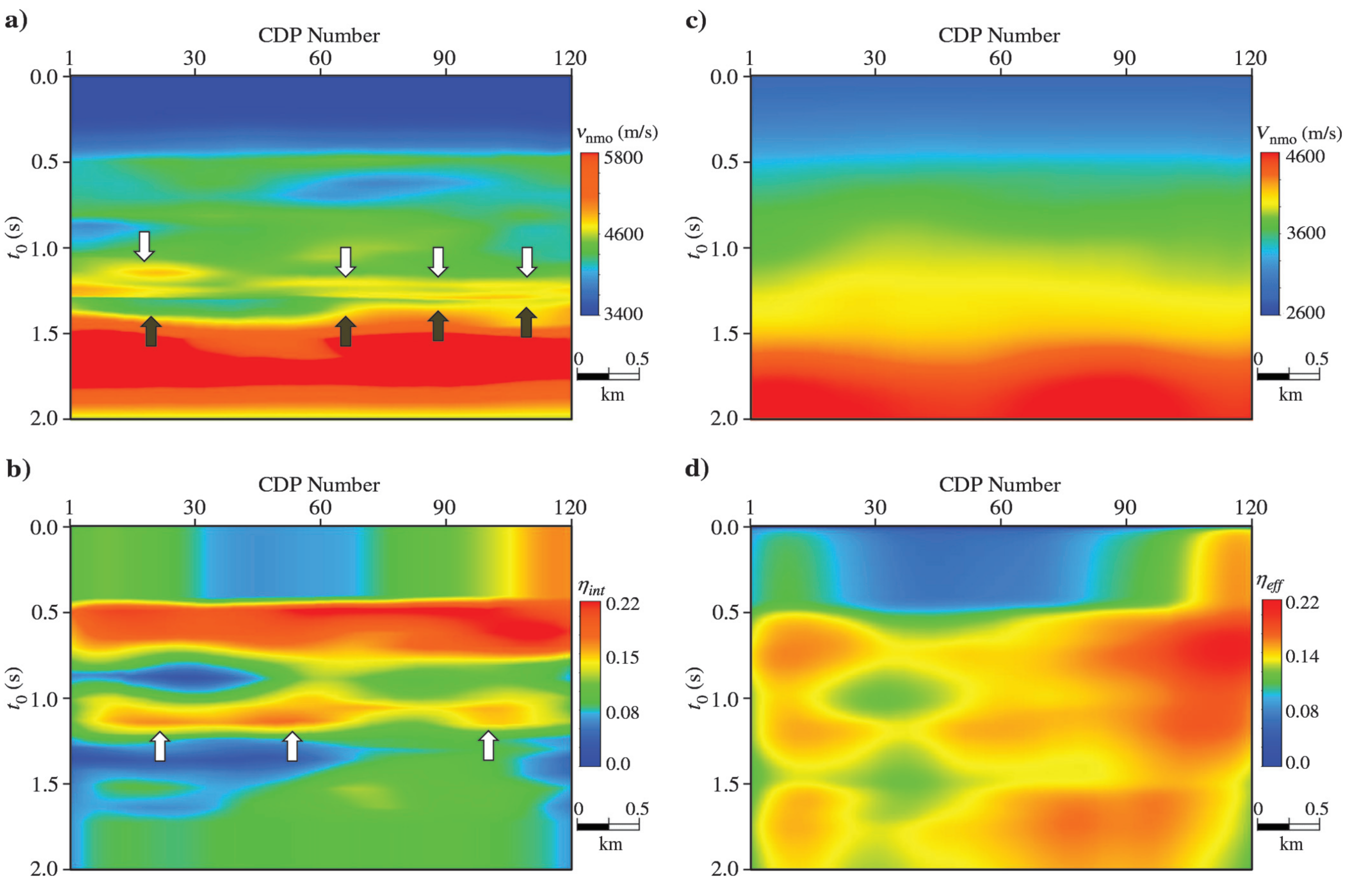

Figure 9. Optimized model results using the workflow shown in Figure 1. During the optimization procedure, we first update the interval NMO velocity: (a) v_{nmo} and (b) η_{int}, then calculate the corresponding (c) rms velocity and (d) effective anellipticity. The optimal interval velocity has higher resolution than the initial interval velocity (Figure 6b).

Barnett Shale–Forestburg Limestone sequences. The velocity increase indicated by the gray arrows corresponds to the Viola limestone. The feature in Figure 9b indicated with white arrows is associated with Barnett Shale, which is known to be a VTI medium. It can be used as a direct anisotropy indicator (Alkhalifah and Rampton, 2001; Abbad et al., 2009).

Note that although the reflection events are flattened by our algorithm, we still cannot use the information contained at large offset due to the serious stretch indicated by the white arrows in Figure 8. At present, MPNMO minimizes the stretch to some extent, but cannot resolve highly interfering and crossing events. Before using this algorithm, we, therefore, apply muting to the time-migrated gathers (Figure 3) that allow wavelets to stretch no more than 180% (Figure 10a). Then, we apply a reverse NMO correction (Figure 10b) on the muted gathers. Finally, we implement the MPNMO algorithm (Figure 10c). Note that MPNMO minimizes the stretch that occurs at the far-offset data when compared with the original time-migrated gathers. Figure 11a and 11b shows vertical slices through the stacked volume from traditional time-migrated gathers after muting and MPNMO-corrected gathers. Note the greater stacked energy (red arrows) and improved resolution (yellow arrow) of the MPNMO results. To better see the improvements, we displayed a magnified part of the stacked section (Figure 12a and 12b) between 1.15 and 1.4 s where our reservoir is located. Those horizons are no longer located at the troughs or peaks on the new stacked section and need reinterpretation. Note the improved resolution indicated by yellow arrows and more continuous reflection events indicated by the red arrow. Unfortunately, the stacking power indicated by the green arrow has lower energy compared with that of conventional. This artifact arises because MPNMO does not properly handle interfering reflections in prestack domain and moves all the interfered energy of current wavelets to the lower reflection events. To quantify the improved resolution, we compare the average amplitude spectra of the stacked data shown in Figure 13. The blue and red curves represent the stacked data using gathers shown in Figure 4 and MPNMO correction (Figure 10c). The MPNMO spectrum obviously has a greater ratio of high to low frequencies.

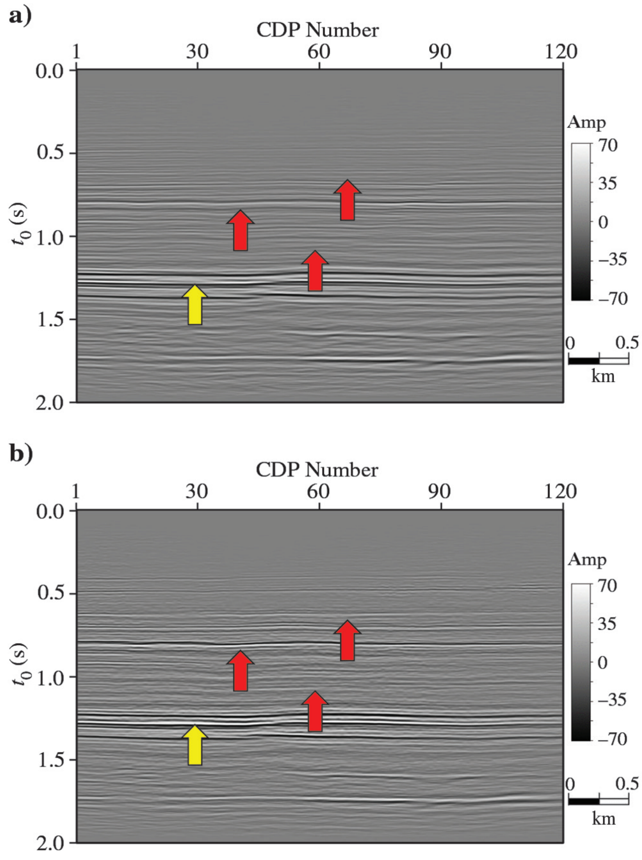

Figure 11. Stacked sections after (a) conventional-migrated gathers with 130% muting criterion and (b) MPNMO correction gathers with 180% muting criterion. The target Barnett Shale lies between $t = 1.1$ and $t = 1.3s$. Note the improved stacking power indicated by the red arrows and vertical resolution indicated by yellow arrow.

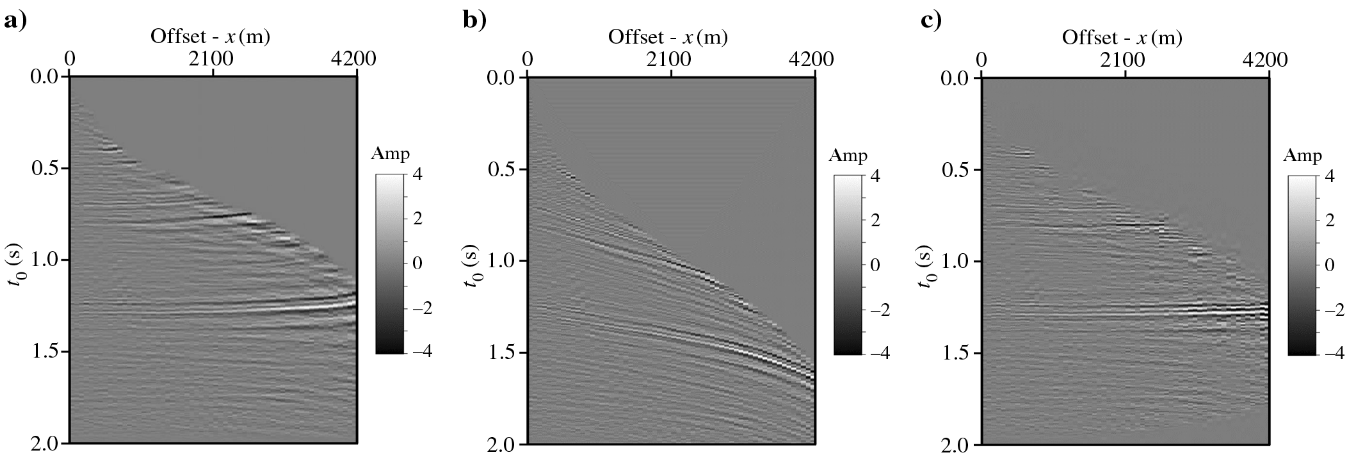

Figure 10. Antistretch processing applied to prestack gathers. Representative gather after (a) muting and (b) reverse NMO correction. The muting is applied on the time-migrated gathers shown in Figure 3 in which the wavelet is not allowed to stretch more than 180%. Reverse NMO is applied to the muted gather. (c) The antistretching processed results. Note, we minimize the stretch at far offsets.

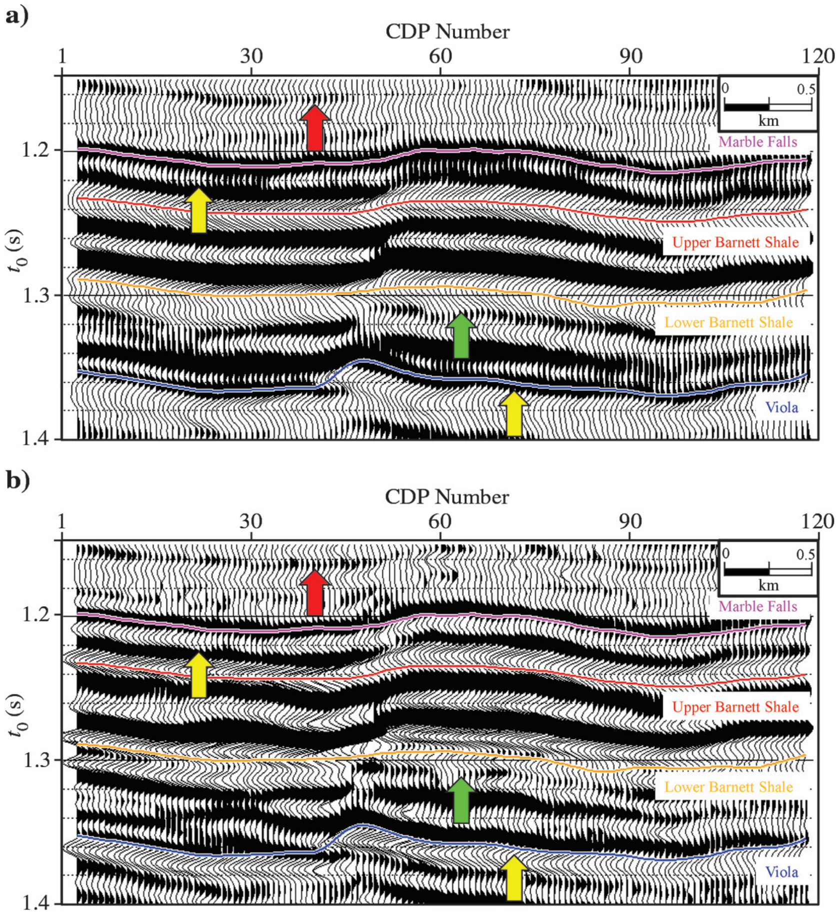

Figure 12. Magnified display of the stacked sections of the target reservoirs. (a) Magnified display Figure 11a at the target reservoirs. (b) Magnified display Figure 11b at the target reservoirs. Note we have more continuous reflection events (red arrows) and improved resolution (yellow arrows).

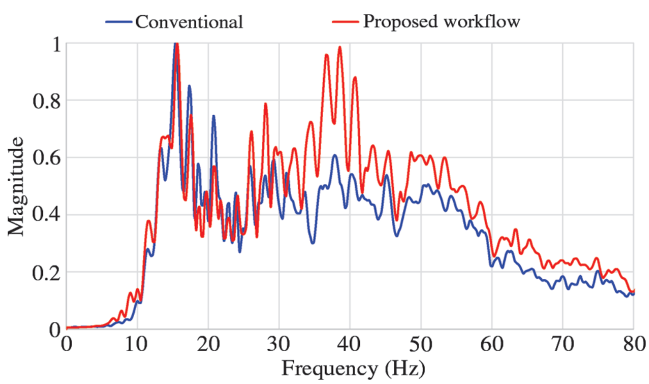

Figure 13. Spectra of stacked section from the conventional (blue) and proposed (red) processing. Note the spectrum of the new stacked section obviously has a greater ratio of high to low frequencies.

CONCLUSIONS

Hockey-stick-like pattern and stretch are the two main issues associated with long-offset data processing. We propose a two-step workflow for maximizing the usage of information contained in far offsets. The first one is an automatic nonhyperbolic velocity analysis to obtain an interval model that gives the maximum stacking power. The interval-model-based search ensures that the optimized model is physically feasible and avoids sudden variations. In our application, the interval velocity has a very good correlation with the reflection events in the stacked section. Unfortunately, the interval anellipticity is ambiguous and needs further comparison with well-log data. Nonhyperbolic velocity analysis can mitigate the hockey-stick-like pattern but not the stretch that appeared at large aperture. MPNMO minimizes the stretch and improves the stacking power and resolution critical for interpreting thin reservoirs. Another advantage benefiting from MPNMO is that more far-offset data are available for subsequent $\lambda\rho$-$\mu\rho$ and AVO inversion.

The proposed methodology has some shortcomings. The algorithm favors flattening stronger reflection events due to their large stacking power and may ignore some weak reflections. Also, it still cannot estimate the nonuniqueness in the solution. There may exist a suite of kinematically equivalent models that exhibit identical moveout curves. The used antistretch algorithm cannot decompose the highly compressed or crossing events. Future work, therefore, includes (1) resolving interfering and crossing events in prestack domain and (2) using well logs as the calibration during the optimization procedure.

ACKNOWLEDGMENTS

The authors thank Devon Energy for permission to use and show their data. We also thank the sponsors of the Attribute-Assisted Seismic Processing and Interpretation Consortium for their guidance and financial support. The final version of this paper benefited tremendously from the comments and suggestions of the associate editors, T. Alkhalifah, K.-J. Lee, and three anonymous referees.

APPENDIX A

DIFFERENTIAL EVOLUTION

The differential evolutionary optimization algorithm used in this paper was initially proposed by Storn and Price (1997). The initial population of DE is randomly generated within the decision space. If the total variable number of the objective function is K, then the nth member at the gth generation can be expressed as:

$$\mathbf{m}_{n,g} \equiv (m^1_{n,g}, \ldots, m^k_{n,g})$$
$$n = 1, 2, \ldots, N; \; g = 1, 2, \ldots, G, \tag{A-1}$$

where N is the population number, G is the total generation, and k is the index for variables. DE exhibits the basic features of any general evolutionary algorithm and is composed of mutation, crossover, and selection.

Mutation

For a given target vector $\mathbf{m}_{n,g}$ at generation g, randomly select three vectors from the population to generate the donor vector as

$$\mathbf{v}_{n,g} = \mathbf{m}_{r_1,g} + F \times (\mathbf{m}_{r_2,g} - \mathbf{m}_{r_3,g}), \tag{A-2}$$

where the indexes, r_1, r_2, and r_3, represent selected integers from $(1, N)$ that are different from n, and F is a user-defined scaling factor.

Crossover

The target vector $\mathbf{m}_{n,g}$ is recombined with the donor vector $\mathbf{v}_{n,g}$ to develop the trial vector $\mathbf{u}_{n,g}$. Elements of the donor vector enter the trial vector with a probability C_r as

$$u_{n,g}^{(k)} = \begin{cases} v_{n,g}^{(k)} & \text{if RAND}(0,\,1) \le C_r \\ m_{n,g}^{(k)} & \text{otherwise} \end{cases}, \tag{A-3}$$

where $n = 1, 2, \ldots, N$, $k = 1, 2, \ldots, K$, RAND(0,1) is the kth evaluation of a uniform random number generator.

Selection

The target vector $m_{n,g}$ is evaluated against the trial vector $u_{n,g}$, with the better model surviving into the next generation as

$$\mathbf{m}_{n,g+1} = \begin{cases} \mathbf{u}_{n,\mathbf{g}} & \text{if } Q(\mathbf{u}_{n,\mathbf{g}}) \le Q(\mathbf{x}_{n,\mathbf{g}}) \\ \mathbf{m}_{n,\mathbf{g}} & \text{otherwise} \end{cases}. \tag{A-4}$$

We repeat implementing equation A-2 to A-4 until the maximum generation G is reached or the convergence rate is smaller than user-defined value.

REFERENCES

Abbad, B., B. Ursin, and D. Rappin, 2009, Automatic nonhyperbolic velocity analysis: Geophysics, **74**, no. 2, U1–U12, doi: 10.1190/1.3075144.

Alkhalifah, T., 1997, Seismic data processing in vertically inhomogeneous TI media: Geophysics, **62**, 662–675, doi: 10.1190/1.1444175.

Alkhalifah, T., 2011, Scanning anisotropy parameters in complex media: Geophysics, **76**, no. 2, U13–U22, doi: 10.1190/1.3553015.

Alkhalifah, T., and D. Rampton, 2001, Seismic anisotropy in Trinidad: A new tool for lithology prediction: The Leading Edge, **20**, 420–424, doi: 10.1190/1.1438964.

Alkhalifah, T., and I. Tsvankin, 1995, Velocity analysis for transversely isotropic media: Geophysics, **60**, 1550–1566, doi: 10.1190/1.1443888.

Biondi, B., and C. Kostov, 1989, High-resolution velocity spectra using eigenstructure methods: Geophysics, **54**, 832–842, doi: 10.1190/1.1442712.

Bolshykh, S. F., 1956, About an approximate representation of the reflected wave traveltime curve in the case of a multi-layered medium: Applied Geophysics, in Russian, **15**, 3–15.

Calderón-Macías, C., M. K. Sen, and P. L. Stoffa, 1998, Automatic NMO correction and velocity estimation by a feedforward neural network: Geophysics, **63**, 1696–1707, doi: 10.1190/1.1444465.

Castle, R. J., 1994, A theory of normal moveout: Geophysics, **59**, 983–999, doi: 10.1190/1.1443658.

Choi, H., J. Byun, and S. J. Seol, 2010, Automatic velocity analysis using bootstrapped differential semblance and global search methods: Exploration Geophysics, **41**, 31–39, doi: 10.1071/EG10004.

Da Silva, M., 2013, Production correlation to 3D seismic attributes in the Barnett Shale, Texas: M.S. thesis, The University of Oklahoma.

De Bazelaire, E., 1988, Normal moveout revisited: Inhomogeneous media and curved interfaces: Geophysics, **53**, 143–157, doi: 10.1190/1.1442449.

Dix, C. H., 1955, Seismic velocities from surface measurements: Geophysics, **20**, 68–86, doi: 10.1190/1.1438126.

Fomel, S., 2009, Velocity analysis using AB semblance: Geophysical Prospecting, **57**, 311–321, doi: 10.1111/j.1365-2478.2008.00741.x.

Fomel, S., and A. Stovas, 2010, Generalized nonhyperbolic moveout approximation: Geophysics, **75**, no. 2, U9–U18, doi: 10.1190/1.3334323.

Key, S. C., and S. B. Smithson, 1990, New approach to seismic-event detection and velocity determination: Geophysics, **55**, 1057–1069, doi: 10.1190/1.1442918.

Kirlin, R. L., 1992, The relationship between semblance and eigenstructure velocity estimators: Geophysics, **57**, 1027–1033, doi: 10.1190/1.1443314.

Larner, K., and V. Celis, 2007, Selective-correlation velocity analysis: Geophysics, **72**, no. 2, U11–U19, doi: 10.1190/1.2435702.

Luo, S., and D. Hale, 2012, Velocity analysis using weighted semblance: Geophysics, **77**, no. 2, U15–U22, doi: 10.1190/geo2011-0034.1.

Montgomery, S. L., D. M. Jarvie, K. A. Bowker, and R. M. Pollastro, 2005, Mississippian Barnett Shale, Fort Worth Basin, north-central Texas: Gas-shale play with multitrillion cubic foot potential: AAPG Bulletin, **89**, 155–175, doi: 10.1306/09170404042.

Neidell, N. S., and M. T. Taner, 1971, Semblance and other coherency measures for multichannel data: Geophysics, **36**, 482–497, doi: 10.1190/1.1440186.

Sacchi, M., 1998, A bootstrap procedure for high-resolution velocity analysis: Geophysics, **63**, 1716–1725, doi: 10.1190/1.1444467.

Siliqi, R., D. Le Meur, F. Gamar, L. Smith, J. P. Touré, and P. Herrmann, 2003, High-density moveout parameter fields V and η: Part one: Simultaneous automatic picking: 73rd Annual International Meeting, SEG, Expanded Abstracts, 2088–2091.

Storn, R., and K. Price, 1997, Differential evolution — A simple and efficient heuristic for global optimization over continuous space: Journal of Global Optimization, **11**, 341–359, doi: 10.1023/A:1008202821328.

Swan, H. W., 2001, Velocities from amplitude variations with offset: Geophysics, **66**, 1735–1743, doi: 10.1190/1.1487115.

Taner, M. T., and F. Koehler, 1969, Velocity spectra: Digital computer derivation and application of velocity functions: Geophysics, **34**, 859–881, doi: 10.1190/1.1440058.

Thomsen, L., 1986, Weak elastic anisotropy: Geophysics, **51**, 1954–1966, doi: 10.1190/1.1442051.

Toldi, L. T., 1989, Velocity analysis without picking: Geophysics, **54**, 191–199, doi: 10.1190/1.1442643.

Van der Baan, M., and J. M. Kendall, 2002, Estimating anisotropy parameters and traveltimes in the τ-p domain: Geophysics, **67**, 1076–1086, doi: 10.1190/1.1500368.

Zhang, B., K. Zhang, S. Guo, and K. J. Marfurt, 2013, Nonstretching NMO correction of prestack time-migrated gathers using a matching-pursuit algorithm: Geophysics, **78**, no. 1, U9–U18, doi: 10.1190/geo2011-0509.1.